Quantifying and Reducing the Operator Effect in LSPIV Discharge Measurements

G. Bodart, J. Le Coz, M. Jodeau, A. Hauet

Quantifying and Reducing the Operator Effect in LSPIV Discharge Measurements

G. Bodart[1,2] , J. Le Coz[2] , M. Jodeau[1], and A. Hauet[3,4]

[1]EDF R&D, LHSV, Chatou, France, [2]INRAE, UR RiverLy, Villeurbanne, France, [3]EDF-DTG, St Martin-le-Vinoux, France, [4]IGE, University Grenoble Alpes—IGE, Grenoble, France

Abstract Operator choices, both in acquiring the video and data and in processing them, can be a prominent source of error in image-based velocimetry methods applied to river discharge measurements. The Large Scale Particle Image Velocimetry (LSPIV) is known to be sensitive to the parameters and computation choices set by the user, but no systematic comparisons with discharge references or intercomparisons have been conducted yet to evaluate this operator effect in LSPIV. In this paper, an analysis of a video gauging intercomparison, the Video Globe Challenge 2020, is proposed to evaluate such operator effect. The analysis is based on the gauging reports of the 15 to 23 participants using the Fudaa-LSPIV software and intents to identify the most sensitive parameters for the eight videos. The analysis highlighted the significant impact of the time interval, the grid points and the filters on the LSPIV discharge measurements. These parameters are often inter-dependent and should be correctly set together to strongly reduce the discharge errors. Based on the results, several automated tools were proposed to reduce the operator effect. These tools consist of several parameter assistants to automatically set the orthorectification resolution, the grid and the time interval, and of a sequence of systematic and automatic filters to ensure reliable velocity measurements used for discharge estimation. The application of the assisted LSPIV workflow using the proposed tools leads to significant improvements of the discharge measurements with strong reductions of the inter-participant variability. On the eight videos, the mean interquartile range of the discharge errors is reduced from 17% to 5% and the mean discharge bias is reduced from −9% to 1% with the assisted LSPIV workflow. The remaining inter-participant variability is mainly due to the user-defined surface velocity coefficient α.

1. Introduction

River discharge is a primary parameter in hydrology. To measure the discharge, various techniques can be used depending on the flow conditions (Rantz, 1982; WMO, 2010). Currentmeters are used in relatively uniform and calm fluvial flows to derive the discharge from velocity measurements throughout a cross-section. Tracer dilution is used in highly turbulent flows to derive discharge from the variation of concentration of a given tracer. The development of innovative streamgauging techniques and guidelines has improved measurement efficiency, performance and safety through the years (Le Coz, 2017). The emergence of Acoustic Doppler Current Profilers (ADCP) was a revolution in streamflow monitoring with the faster, safer and more accurate acquisition of stream velocities and depths thanks to specific Doppler sonars mounted on moving boat (Rowe & Young, 1979; Simpson & Oltmann, 1993). Particularly, the ADCP facilitate the discharge measurement of very large rivers such as the Amazon at Obidos which can be gauged in a few hours instead of 3 days with currentmeters (Callède et al., 2003). More recently, the development of non intrusive surface velocimetry techniques such as surface velocity radars, cf. pioneering works of Costa et al. (2000), and imagery, cf. pioneering works of Fujita et al. (1998), Creutin et al. (2003), has enabled flood discharge measurements in extreme conditions, especially fast-flowing and highly turbulent flows. These contactless methods ensure safe measurements for example, from a bridge for surface radars or from river side surveillance camera or smartphone, drone and satellite for imagery. They allow to capture more discharge measurements at high flows, which helps to reduce the extrapolation uncertainty of stage-discharge rating curves used to compute discharge time series from stage records (Kiang et al., 2018). Image-based velocimetry methods were built on techniques initially developed for experimental fluid dynamics. For instance, the pioneer Large Scale Particle Image Velocimetry (LSPIV) (Fujita et al., 1998) was based on the well-known Particle Image Velocimetry (PIV) (Adrian, 1991). The displacements of surface patterns (e.g., turbulence patterns, boils, debris, foam, specular reflections) usually illuminated by natural sun light are determined between consecutive frames. A preliminary orthorectification step is needed to account for

image distortion caused by oblique views and to transform image coordinates to real-world coordinates (Le Coz, Renard, et al., 2021).

With this progress in the streamgauging techniques, the measurements have become more efficient but also more complex in terms of hardware and software. The hardware complexity can lead to measurement errors and the software complexity can increase the operator effect due to the specific expertise expected from the user (Detert, 2021). Each new technique also comes with particular sensitivity to the environmental conditions, depending on its operating principle. All these limitations have to be studied to ensure the reliability of the measurement, necessary to the operational deployment of the technique. For instance, the operational deployment of the ADCP followed several steps with first the validation of the method against precise references in various laboratory and field conditions (Oberg & Mueller, 2007), then the quantification of the measurement uncertainties through specific computation frameworks (Despax et al., 2023; González-Castro & Muste, 2007; Moore et al., 2017) supplemented by repeated-measures experiments (a.k.a. intercomparisons) (Despax et al., 2019; Le Coz et al., 2016). This leads to the elaboration of procedures (ISO, 2021a; Mueller et al., 2013; WMO, 2010) and the development of software tools such as QRev (Mueller, 2016). The ADCP softwares from manufacturers became more and more assisted with automated settings requiring less parameters and expertise from the user. More recently, quality assurance (QA) and quality control (QC) processes have been formalized into the QRevInt software (Lennermark & Hauet, 2022) to ensure measurement reliability and to quantify the uncertainty. Now, the ADCP technique can be regarded as fully operational.

Several image-based methods including LSPIV have been validated for surface velocity determination, for example, (Brevis et al., 2011; Eltner et al., 2019; Fujita et al., 2007; Hauet et al., 2008; Leitão et al., 2018; Perks et al., 2016). Among others, LSPIV is known to have a large number of parameters and to be sensitive to the operator choices in terms of parameter settings, cf. (Detert, 2021; Pearce et al., 2020). But unlike ADCP, no systematic studies based on data sets with discharge reference, for example, (Perks et al., 2020), nor intercomparisons have been conducted yet to evaluate the influence of the operator settings on the LSPIV measurement. Overall, image-based discharge measurement still lacks systematic validation, homogeneous procedures, and complete uncertainty computation framework. Only few contributions can be found with guidelines (USGS, 2022; WaMSTeC, 2021) and uncertainty computation methods (Kim et al., 2007; Le Coz, Renard, et al., 2021; Rozos et al., 2020; Schweitzer & Cowen, 2022) which are still incomplete as not all uncertainty sources, especially the operator effect, are covered.

The objective of this paper is to quantify and reduce the operator effect due to data processing in LSPIV discharge measurements. What will be called "the operator effect" in the rest of this paper does not cover other operator effects in the field operations (site selection, video recording, topography measurements, etc.) nor operator-independent effects (flow conditions, illumination, fixed parameters and algorithms specific to the software used, etc.). The resulting inter-operator reproducibility is studied through the LSPIV outputs of a video streamgauging intercomparison. Random repeatability, certainly negligible compared to inter-operator reproducibility, is not quantified as each participant provided only one result per video.

The Fudaa-LSPIV software (Le Coz et al., 2014), presented in Section 2, is used for the study as it proposes a standalone, complete and widely used implementation of LSPIV. The video gauging intercomparison, namely the Video Globe Challenge 2020 (VGC2020) (Le Coz, Hauet, & Despax, 2021), presented in Section 2, consists of eight videos coming with a discharge reference measurement with uncertainty estimate, and with the discharge results of nearly 25 participants. The eight cases represent typical video streamgauging situations covering various environmental conditions, types of flows and error sources. The framework applied to analyze the VGC2020 and quantify the operator effect (i.e., parameters sensitivity) is presented in Section 2. Parameter assistant tools and automated filters are proposed in Section 3 to reduce the operator effect in the context of discharge measurement. These new automatic parameter settings and filters, not available to the participants, intend to produce discharge results as good as what the best participants were able to get by manually setting the limited options offered by the current version of Fudaa-LSPIV, based on their individual expertise. The sensitivity analysis of the LSPIV method based on the VGC2020 data set is presented in Section 4. New LSPIV workflows for discharge estimation using parameter assistants and automated filters are proposed and evaluated on the VGC2020 data set in Section 4. The findings and limitations of the presented work are discussed in Section 5.
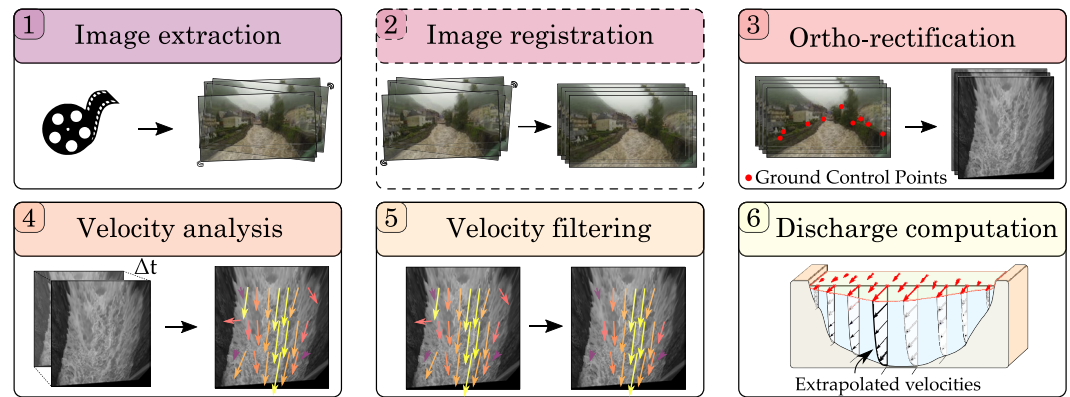
Figure 1. Illustration of the main steps of the Large Scale Particle Image Velocimetry procedure.

2. LSPIV Software, Intercomparison Data, and Analysis

2.1. The Fudaa-LSPIV Software

Fudaa-LSPIV (Jodeau et al., 2022; Le Coz et al., 2014) is a free and open source software (link provided in the Open Research section) that embeds all the steps of LSPIV through a user-friendly interface. Its main steps are summarized in Figure 1 and detailed hereafter. The ffmpeg library (Tomar, 2006) is used to extract images from a video file. The start and end times of the sequence to be extracted have to be set. The framestep corresponds to the down-sampling factor (integer) of the video framerate for the image sequence extraction. For instance, with a framestep of N, only one every N images will be extracted. As a consequence, the time interval of the generated sequence will be N times longer than the time interval of the original video. A framestep of 1 means that all the images in the videos are extracted, so the time interval and the framerate remain the same as in the original video.

Fudaa-LSPIV includes a specific image registration algorithm, only required in case of camera movements. The image sequences are stabilized based on the unmoving part of the image, that is, out of the flow area. The flow area and a geometric transformation model for registration are defined by the user. The method uses the SURF algorithm as implemented by Oyallon and Rabin (2015).

The orthorectification step is used to build a physically scaled ortho-image of the water surface. Orthorectification includes camera calibration and ortho-image construction. Camera calibration aims to estimate the camera intrinsic parameters (focal length, optical center, skewness factor) and extrinsic parameters (camera location and orientation). Several methods can be found for camera calibration, see Zhang (2000). An implicit calibration method based on Ground Control Points (GCPs) is implemented in Fudaa-LSPIV, cf. (Jodeau et al., 2008). The "3D" orthorectification procedure requires a minimum of six GCPs and the water level. The "2D" orthorectification procedure requires four GCPs located at the water surface elevation. In case of a perpendicular viewpoint, that is, nadir views, ortho-images can be obtained by simply scaling the images. Scaling distances have to be identified at the water surface elevation. The resolution and the limits of the ortho-image have to be specified by the user. The resolution defines the physical size of a pixel in meters. The limits of the ortho-image, in fact the minimum and maximum x and y metric coordinates, define the size of the ortho-image.

The velocity analysis is performed at fixed points, distributed in the ortho-images. The measurement points are defined by the user through a grid. Fudaa-LSPIV allows to configure various grid point densities on the image. The displacements are determined between consecutive frames based on a pattern matching algorithm with normalized cross-correlation metrics, cf. (Muste et al., 2008). The Interrogation Area (IA) defines the size of the (square) block to be matched and the Searching Area (SA) defines the scanned zone on the next frame, that is, the area of the possible displacements of the center of the IA.

After the velocity analysis, instantaneous velocity fields are available at each time step. Spurious vectors can be filtered out. In the current version of Fudaa-LSPIV (Jodeau et al., 2022), some basic filter options are proposed: a velocity result is rejected if the peak normalized cross-correlation metrics, the velocity magnitude or the velocity components fall outside user-defined permissible ranges. Velocity filtering is an important and sensitive step of

image-based methods and these two simple filters may be limited. The time-averaged velocity field is computed from the filtered velocity fields.

Finally, the discharge through a given bathymetric transect can be obtained using the velocity-area method (ISO, 2021b). The depth-averaged velocities are determined at each point of the transect. An area defined by an ellipse is considered around each point. The three nearest time-averaged velocities contained in this area are averaged with an inverse distance weight to obtain the transect surface velocity. If no time-averaged velocities are found in the ellipse then the transect surface velocity is extrapolated. The extrapolation uses the available transect surface velocities and considers a linear Froude number variation between them (cf. the Fudaa-LSPIV user manual, Jodeau et al., 2022). The depth-averaged flow velocities $\bar{v}$ are computed from the transect surface velocities v_{surf} and the depth-averaged to surface velocity ratio, a.k.a. surface coefficient α, set by the user so that: $\bar{v} = \alpha v_{surf}$. A default coefficient of $\alpha = 0.85$ is usually set for river flows assuming a logarithmic vertical velocity profile and typical bed roughness (Costa et al., 2000). But α can vary significantly depending on the site (i.e., river section and hydraulic conditions) (Biggs et al., 2021; Le Coz et al., 2010; Welber et al., 2016). The total discharge is computed using the mid-section method (ISO, 2021b). A gauging report can be exported to summarize the calculation parameters and the discharge results.

2.2. The Video Globe Challenge 2020

The VGC2020 (Le Coz, Hauet, & Despax, 2021) is a video streamgauging intercomparison which involved between 22 and 26 participants during the COVID-19 lock-down of spring 2020. The participants had various levels of experience with video streamgauging, from beginners to experienced users. Several image-based velocimetry techniques and software were used including mainly Fudaa-LSPIV but also SSIVSuite (Leitão et al., 2018), PIVlab (Thielicke & Stamhuis, 2014), OpyFlow (Rousseau, 2019) and manual processing. Only the LSPIV analyses are considered in this study as not enough measurements with other softwares are available for the intercomparison. The level of information and training of the participants to the VGC2020 was typical of actual users of Fudaa-LSPIV, open-source and released freely with general instructions (user manual, tutorials, classes). In the intercomparison experiment, the necessary data and information (e.g., photos, bathymetry transect, vertical velocity profiles if any, etc.) were provided with each video, but no specific instructions or advice were provided in order not to influence the operator choices. The results of each video were reported with explanations of the main errors and tricks before the next video was submitted to the participants, so they could improve their understanding of the method and software.

Once again, the exercise is representative of real practice, and the results are meaningful in showing that instructions and training are not enough to prevent a lot of users from making mistakes and getting inaccurate discharge results. Hence the importance of developing and implementing the proposed tools for automatic or assisted parameter settings and filters.

The eight videos of the VGC2020 (cf. Figure 2) were provided by various hydrological services in France (EDF and DREAL Auvergne-Rhône-Alpes), Australia (Mark Randall, DNRME Queensland) and Norway (NVE) that had used them to this end. These videos were selected not for their difficulty but as they are typical of real video-based streamgauging conditions in the field and as they come with site information, discharge references and uncertainty estimates, mainly based on ADCP measurements, exceptionally from a stage-discharge relation or tracer-dilution measurements. They represent typical and sometimes challenging operating situations encountered in operational practice. The image conditions are often far more difficult for LSPIV than laboratory experiments with much better seeding and illumination, of course. However, all the videos were considered to be useable for correct LSPIV discharge measurements.

The range of river widths covered, from 3.5 to 190 m, is typical of applications in small to medium-sized rivers, even though the technique is applicable to smaller or bigger rivers. Viewpoints vary from low-angle views to vertical (nadir) views. A variety of orthorectification methods can be found with different types and distribution of GCPs. The water surface aspects vary due to different lighting, flow conditions and water aspect. As typical in hydrometric applications, especially in flood situations, no artificial tracer is added to the flow and velocity is measured from the apparent movement of free-surface turbulent-driven patterns or foam. This limits the accuracy of the velocity and discharge results, but the experience shows that such naturally-occurring tracers can be good enough for hydrometric purposes. Artificial seeding using cornstarch (biodegradable) packing beads is used only
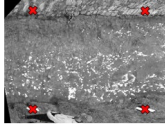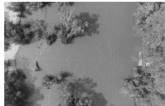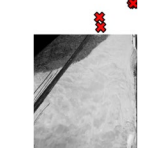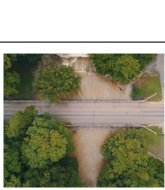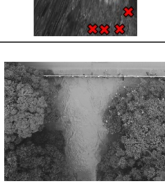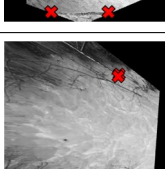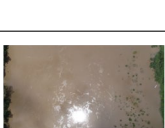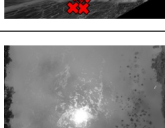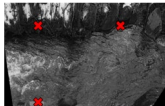
Case	River	Source image +GCPs (red crosses)	Video duration	Video framerate	River width	Ortho-rectif. mode	Ortho-image +GCPs (red crosses)	Surface velocity (min - max)	Error sources	α	$Q_{ref} \pm U_{ref}$ (method)
1	Vence, France		13 s	25 fps	6 m	2D		0.5 - 0.8 m s^{-1}	- Water transparency - Variable tracer density	To be estimated	1.26 m^3/s ± 12.4% (ACDP, Oursin)
2	West Normanby, Australia		25 s	30 fps	55 m	Scaling (drone)		0.1 - 1.8 m s^{-1}	- Shadows - Vegetation - Glares - Variable tracer quality	0.85	107.95 m^3/s ± 5.5% (ACDP, Oursin)
3	Séran, France		11 s	30 fps	16 m	3D		0.9 - 2.5 m s^{-1}	- Low angle - Camera shaking - Backwater from bridge	To be estimated	55.16 m^3/s ± 8.7% (ACDP, Oursin)
4	Russel, Australia		24 s	30 fps	40 m	Scaling (drone)		1.7 - 2.2 m s^{-1}	- Large occlusions (canopy)	0.92	139 m^3/s ± 15% (Stage-discharge, estimate)
5	Storåne, Norway		14 s	30 fps	19 m	2D		0.9 - 1.7 m s^{-1}	- Wind - Low angle - Variable tracer quality (reflections) - Camera shaking	1.0 (wind)	19.7 m^3/s ± 10% (ACDP, estimate)
6	Groin, France		11 s	30 fps	9 m	3D		0.7 - 3.6 m s^{-1}	- Occlusions (vegetation) - Poor GCPs distribution	To be estimated	53.74 m^3/s ± 9.3% (ACDP, Oursin)
7	Herbert, Australia		22 s	30 fps	190 m	Scaling (drone)		0.3 - 2 m s^{-1}	- Glares - Vegetation	0.95	962.8 m^3/s ± 5.3% (ACDP, Oursin)
8	Finsal-bekken, Norway		13 s	30 fps	3.5 m	2D		0.2 - 1.2 m s^{-1}	- Instable tracers - Variable tracer quality	To be estimated	0.636 m^3/s ± 5% (Dilution, Suny)

Figure 2. Presentation of the eight cases of the Video Globe Challenge 2020 with information about the river and the video. The mean and maximum surface velocities are extracted from the velocities at the transect obtained from a correct Large Scale Particle Image Velocimetry measurement.

in the first video. Tracer density and quality vary across the eight videos. In the videos 2, 3, 4, and 6 the water surface is opaque with tracers homogeneously distributed which is ideal for image velocimetry. In the videos 5, 7, and 8 the tracers density vary across the river due to surface reflections (video 5 and 7) or surface roughness (video 8). Several typical error sources can be found across the eight cases including surface reflections, glares, occlusions or water transparency. The coefficient α varies from case to case. It was either given or had to be estimated based on information on vertical velocity profiles provided from ADCP or currentmeter measurements conducted at the same site.

Figure 3. Fudaa-Large Scale Particle Image Velocimetry results of the Video Globe Challenge 2020 video-based discharge measurement intercomparison: (a) Distributions of the percent deviations ΔQ_j between the measurements and the discharge references of video j, with n_p the number of participants and U_{ref} the 95% uncertainty of the discharge reference and (b) decomposition of the discharge errors ΔQ_j over the N_v videos processed by each participant.

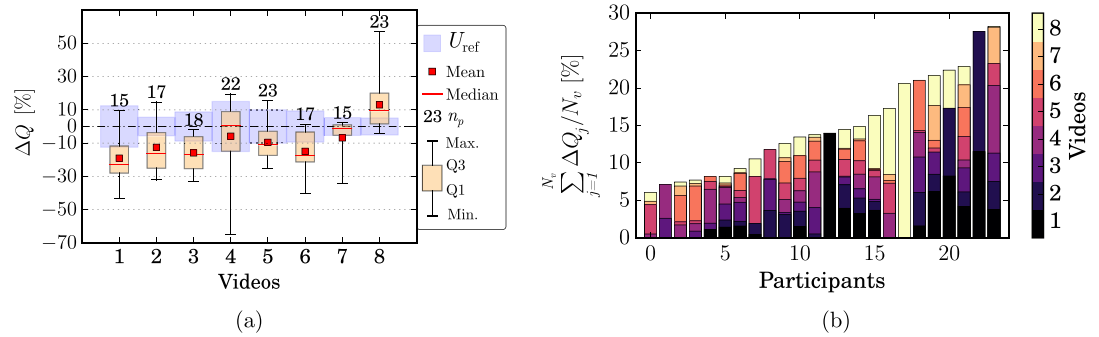The participants using Fudaa-LSPIV submitted detailed gauging reports including LSPIV discharge results and several parameters (participants LSPIV parameters are shown in Supporting Information S1 attached to this article). The scatter in user-defined parameters (framestep, IA and SA sizes, sequence duration and alpha coefficients) was substantial. Except when alpha was given to participants (videos 2, 4, 5, 7), participants selected alpha values over a realistic range, typically 0.8–0.9 except for video 3 (flow upstream of a nearly submerged bridge). Then, the participants selected higher values (0.85–1.0, median 0.95) which made sense with the provided vertical velocity profiles measured with an ADCP. A vast majority of participants activated the minimum peak correlation filter. In the last versions of Fudaa-LSPIV, this filter is activated by default with a threshold of 0.4. Nearly half of the time, the threshold was set lower (which is very risky), and only about 20% of the time it was set to a higher threshold value (which is safer as it is more selective). The minimum velocity magnitude filter was often used, sometimes with rather high thresholds, certainly to discard spurious velocity vectors that could not be discarded by other means (better parameters or filters). The maximum velocity magnitude filter was seldom used (about half of the time only), and usually with relatively high thresholds. This filter was certainly used to discard a few very high velocity results that may have been filtered more directly by limiting the downstream SA size.

The discharge results are compared with the discharge reference and its uncertainty in Figure 3a. The discharge reference come from ADCP measurements for videos 1, 2, 3, 5, 6, and 7 and from a dilution measurement for video 8. The 95% uncertainty of the reference U_{ref} is computed from the measurement data using the Oursin method (Despax et al., 2023) for ADCP measurement and the Suny method (Hauet et al., 2020) for the dilution method. For video 5, the wind acting on the surface impacts the vertical velocity profile and thus the top layer extrapolation of the ADCP discharge measurement. The 5% uncertainty computed with the Oursin method seems to neglect the surface extrapolation uncertainty. An estimated uncertainty of 10% is used instead to take into account the surface extrapolation uncertainty. No discharge measurement data are available for the video 4. The reference discharge is obtained from the stage-discharge rating curve at the measurement location. The upper part of the stage-discharge rating curve is used to obtain the reference discharge. This part shows higher uncertainties as it is built with fewer gaugings. As a consequence, a 95% uncertainty of 15% is estimated on the discharge reference.

The LSPIV discharge measurements are largely scattered with substantial individual deviations. The discharge error ΔQ is defined as the percent difference between the measured discharge Q and the discharge reference Q_{ref}:

$$\Delta Q = \frac{Q - Q_{\text{ref}}}{Q_{\text{ref}}} \cdot 100 \tag{1}$$

For a given video, the interquartile range of the discharge errors ΔQ varies from 6% to 24% across the participants with a mean value of 17%. Large deviations from the discharge references are observed, except for videos 4, 5, and 7 (cf. Figure 3a). The level of experience in LSPIV strongly affects the parameter choices, thus the discharge errors. Participants with limited experience tend to obtain large (>20%) discharge errors (cf. Figure 3b) mainly due to setting mistakes. Experienced users performed better with mean discharge error smaller than 10%.

The discharge errors also seem to be influenced by specific error sources. A tendency to underestimate the discharge is observed in videos containing areas with poor surface tracers or occlusions, for example, videos 1,
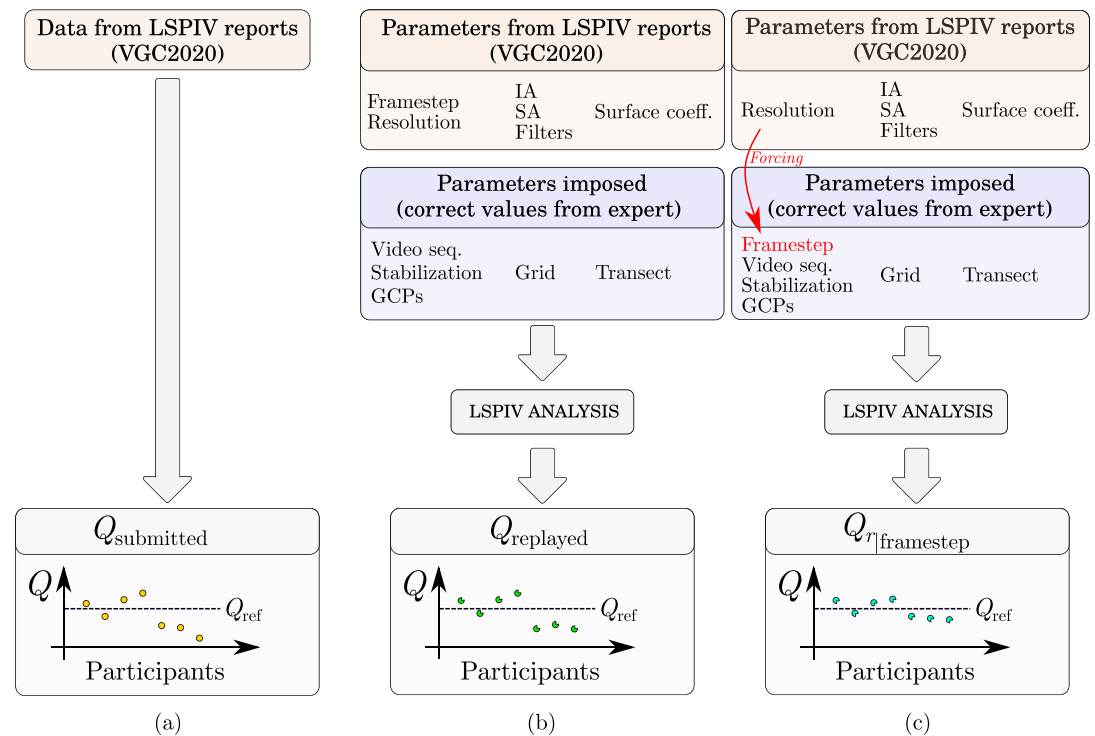
Figure 4. Reprocessing of the Video Globe Challenge 2020 (VGC2020) data set: (a) Discharges $Q_{submitted}$ measured by the VGC2020 participants, (b) Discharges $Q_{replayed}$ replayed with the users parameters from the Fudaa-Large Scale Particle Image Velocimetry gauging report and fixed parameters, and (c) Discharges $Q_{r|x}$ replayed with some user parameters x forced at a correct value.

2, and 5. With an appropriate amount of surface tracers through space and time, the results are less scattered, for example, in videos 4 and 7. However, the causes for several substantial discharge errors in videos 3 and 6 remain unexplained at first glance.

2.3. Reprocessing of the VGC2020 Data Set

In order to quantify the sensitivity of the LSPIV method to its parameters, we have reprocessed and investigated the Fudaa-LSPIV measurements of the VGC2020. For each video, 15 to 23 participants using Fudaa-LSPIV had submitted their results through streamgauging reports issued from the software. Despite the substantial scatter of the parameters chosen by the participants, this sample is too small to ensure a correct coverage of all the possible parameter values. Hence, classical sensitivity analysis schemes such as Sobol indices are not relevant. In addition, the setup of the LSPIV method is complex with inter-dependent parameters and case-dependent parameters such as spatio-temporal sampling, grid points and filters. The computational time can vary substantially with the parameters used, from a few seconds to 1 hour per analysis in case of very dense grid and large IA. Consequently, it would be time-consuming to run LSPIV computations massively in order to evaluate all the possible setting combinations. A simplified framework is preferred with less but meaningful LSPIV computations. The LSPIV measurements are reprocessed over identical temporal slots and at identical grids and transects, facilitating the comparison of the LSPIV velocities and discharges.

The Fudaa-LSPIV streamgauging reports submitted by the participants of the VGC2020 contain the discharge measurements $Q_{submitted}$ initially computed by the participants (cf. Figure 4a). The $Q_{replayed}$ data set consists of LSPIV computations run with the user parameters from the streamgauging reports and the missing parameters fixed (cf. Figure 4b). The reports indeed provide most of the parameters used in the LSPIV analysis (framestep, ortho-image resolution, IA, SA, filters and surface coefficient). We had to fix other parameters not included in the reports: the video sequencing, the image registration parameters, the GCPs coordinates and the coordinates of the velocity grid points. In particular, for each video we have extracted the same 9 s-long sequence displaying the maximum amount of visible tracers at the water surface for all the participants. We applied

Table 1
Summary of Forced Parameters, Expert-Assessed for Each Video, for Re-Analyzing the Results of the Participants to the Video Globe Challenge 2020, With r the Peak Correlation (Dimensionless), n the Velocity Magnitude (m/s), v_x and v_y the Velocity Components (m/s) Along x and y Axes, and α the Surface Coefficient (Dimensionless)

Videos	1	2	3	4	5	6	7	8
Framestep	≥3	≥6					≥5	
Grid					Trunc.			
Filter r	$r > 0.65$	$r > 0.5$		$r > 0.6$			$r > 0.6$	$r > 0.45$
Filter n	$2 > n > 0.1$	$3 > n > 0.1$		$3.5 > n > 0.1$			$2.5 > n$	$2 > n > 0.1$
Filter v_x	$v_x > 0$						$-0.5 < v_x < 0.5$	
Filter v_y		$v_y > 0$		$v_y > 0$			$v_y > 0$	
α			1.06					
GCPs image coor.						Other pointing		

Note. Empty cells mean that the participant-defined parameters were not modified.

image stabilization to videos 3, 5, 6, and 8. We set the same computational grid around the transect, for all the participants, excluding points falling out of the flow area or in vegetated areas. The obtained grid points for reprocessing LSPIV analysis are shown on the ortho-images in Supporting Information S1 attached to this article. The bathymetric transects used for discharge computation are those provided to the participants in the VGC2020 datafiles.

Other data sets are created based on the same replaying scheme but forcing some parameters identified as sensitive, other parameters being kept as defined by each participant. The forced values (Table 1) correspond to appropriate sets of parameters estimated by an expert assessment of the conditions of each video. Forcing the framestep ensures sufficiently long displacements (i.e., larger than 3 pixels) from frame to frame. The framestep is forced only if the participant setting is below the correct value proposed in Table 1. For video 5, the truncated grid only covers the textured half of the flow. The forcing on the filters embeds the peak correlation threshold and the velocity thresholds. The specific surface coefficient of video 3 has been computed from the reference ADCP vertical velocity profile. The obtained discharge results are noted $Q_{r|x}$ with x the forced parameter (cf. Figure 4c). For these $Q_{r|x}$ data sets, the video sequencing, GCP coordinates, stabilization parameters and grid points are the same as those of the Q_{replayed} data set. To evaluate the inter-dependency between the parameters the forcing is applied to several parameters together or one at a time.

The evaluation of the LSPIV errors considers the discharge error ΔQ (Equation 1) and the Root Mean Square Relative Error η defined as a relative measure of the error between n discharge measurements Q_i and the discharge reference Q_{ref}:

$$\eta = \sqrt{\frac{1}{n} \cdot \sum_{i=1}^{n} \left(\frac{Q_i - Q_{\text{ref}}}{Q_{\text{ref}}} \right)^2} \cdot 100 \qquad (2)$$

3. Methods for Reducing the Operator Effect

3.1. Automatic Definition of LSPIV Parameters

Several automatic parameter definition tools are proposed to set the orthorectification resolution (P_0), the grid points (P_1), the size of the SA (P_2) and the framestep (P_3). These tools should require minimal input from the user. They can use the information from user-provided data such as GCPs and transect data. The principles of the automatic parameter definition tools are presented in Figure 5 and explained in detail in the next paragraphs.

Tool P_0 sets the finest ortho-image resolution (in m/pix) allowed by the source image resolution in the region of interest. The source image resolution in the region of interest is obtained from the GCPs metric and pixel coordinates. To determine the optimal resolution r_{ortho}, P_0 computes the mean source image resolution in the area of interest defined as the convex hull of the GCPs positions (cf. Figure 5a). The number of pixels N_p that fall into
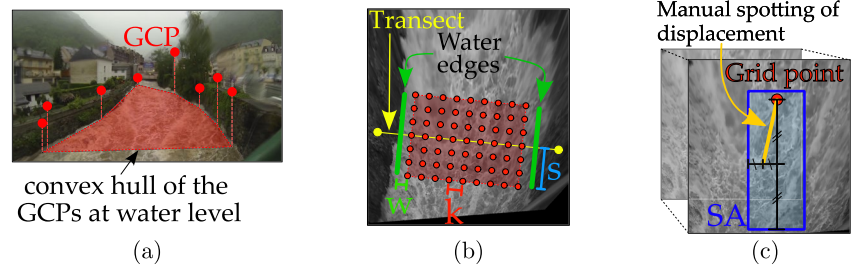
Figure 5. Principles of the proposed automatic parameter definition tools (a) P_0 for orthorectification resolution using the Ground Control Points data, (b) P_1 for grid points using the transect data, with W the distance in the spanwise direction between the grid area and the water edges, S the distance in the streamwise direction between the grid area and the transect and k the sampling distance of the grid points and (c) P_2 for the Searching Area size using manual spotting of the displacement. See text for details.

this polygon and the metric area A_m of the polygon are determined. The mean source image resolution, in meters per pixel, can be obtained from N_p and A_m so that:

$$r_{\text{ortho}} = \sqrt{\frac{A_m}{N_p}} \tag{3}$$

Tool P_1 defines a high-density computational grid in the flow area around the transect. A high density of grid points has to be set to enforce the spatial coherency of the results in their local neighborhood, that is, to reduce spatial velocity gradients. The grid area is centered on the wetted part of the transect, computed using the water level information (cf. Figure 5b). In the spanwise direction, the grid area extends up to a distance k equal to the IA size from the water edges. In the streamwise direction, the grid area extends upstream and downstream from the transect by a distance s equal to 1/30th of the river width, with a minimum value of 1 m to ensure sufficient amount of grid points for small streams. A sampling distance k of 15 pixels between the grid points is set by default. If the grid contains more than 1,000 points, the grid is down-sampled by two to make sure the execution time remains reasonable. Indeed, the default grid definition criteria may lead to very large grids in case of wide rivers and/or highly resolved images (e.g., video 7 with 190 m river width and 4 K resolution, cf. Figure 2).

Tool P_2 defines the size of the SA based on the manual spotting of one or a few displacements between consecutive ortho-images in high flow velocity areas (cf. Figure 5c). The largest velocity component among v_x or v_y defines the streamwise direction (x or y) and its sign defines the flow direction (upstream/downstream). The SA sizes in the downstream and upstream directions are defined as twice the maximum streamwise positive displacement and as one pixel, respectively. In the spanwise direction, the SA sizes are defined as twice the maximum spanwise displacements in both ways.

Tool P_3 sets an optimal framestep based on the results of preliminary LSPIV computations run with iteratively increased framestep. Long frame-to-frame pixel displacements reduce the resolution uncertainty and the impact of sub-pixel intrepolation errors. They also help to segment actual flow velocities from spurious near-zero velocities. But a too large framestep may lead to erroneous results due to the stronger deformation of the surface patterns between consecutive frames. To ensure a good balance, the optimal framestep is defined as the smallest framestep ensuring that 75% of the displacements across the grid points are greater than 3 pixels. LSPIV analysis is applied iteratively to the first two images of the sequence with an IA of 40 pixels and the SA and grid defined by tools P_2 and P_1. A minimum correlation peak threshold of 0.3 and a minimal displacement magnitude threshold of 0.75 pixel are set to remove spurious vectors (especially near-zero velocities). A framestep of 1 (all images kept) is applied first and increased until the first quartile of the displacement distribution is greater than 3 pixels.

3.2. Automatic Filters for LSPIV

Several filters are proposed to enhance the performance of LSPIV discharge measurements assuming a quasi-unidirectional and steady flow around the transect: a spatial coherency filter (F_0) based on the median test introduced by Westerweel and Scarano (2005) and widely used in laboratory PIV applications, a correlation peak width filter (F_1), a velocity temporal distribution filter (F_2), a streamwise velocity dispersion filter (F_3), an angular dispersion filter (F_4), and the computation of the time-median velocity field instead of the time-average
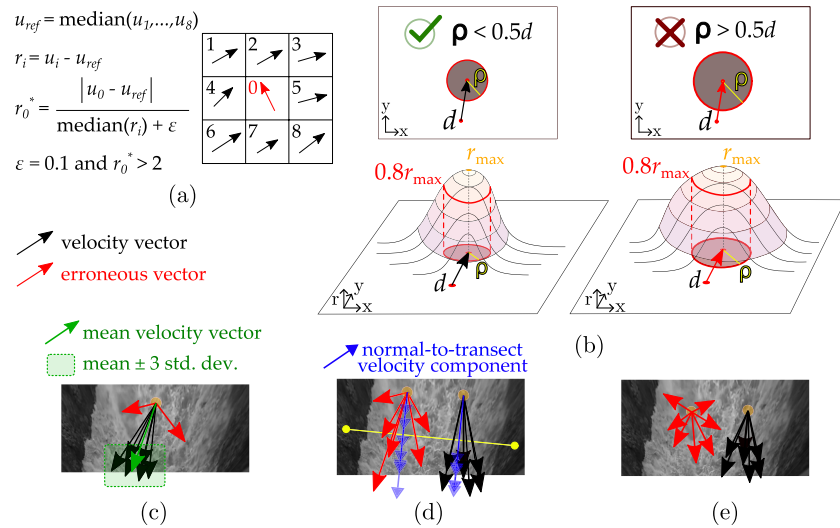
Figure 6. Principles of the proposed automatic filter tools: (a) spatial coherency filter F_0 using the median test (Westerweel & Scarano, 2005) applied on the velocities u of the eight neighbors with r_0^* the normalized residual threshold and ϵ the acceptable fluctuation level, (b) correlation peak width filter F_1 using the correlation field with measured correlation r to evaluate the radius ρ of the peak width at 80% compared to the velocity magnitude d, (c) velocity temporal distribution filter F_2 using the mean and standard deviation of the velocities computed at a point, (d) streamwise velocity dispersion filter F_3 using the normal-to-transect velocities computed at a point, (e) angular dispersion filter F_4 using the velocities computed at a point. See text for details.

(F_5). Like the parameter automatic definition tools, the filters should require the smallest inputs from the user. The principles of the automatic parameter definition tools are presented in Figure 6 and explained in detail in the next paragraphs.

Filter F_0 applies the median test (Westerweel & Scarano, 2005) to ensure the local spatial coherency of the velocity vectors, using the recommended values for the normalized residual threshold $\left(r_0^* > 2\right)$ and the acceptable fluctuation level ($\epsilon = 0.1$ pix). See Figure 6a for the mathematical definition of r_0^*. The nearest 8 neighbors of a given velocity grid point within a maximal distance of 5 m are identified using a kd-tree (Bentley, 1975). The advantage of the kd-tree is that it can rapidly identify the nearest neighbors even in case of non-regular grids as used for LSPIV.

Filter F_1 evaluates the width of the correlation distribution around the correlation peak and compares it to the measured displacement magnitude to keep only robust measurements with sharp correlations peaks. Indeed, a wide correlation distribution occurs in case of poorly textured patterns due to low tracer density. The area A_r (in squared pixels) around the peak with a correlation r greater than 80% of the maximum r_{max} is measured with a flood fill algorithm (Foley & Van Dam, 1982) applied to the correlation field (cf. Figure 6b). The algorithm begins from the peak location and runs with the condition $r > 0.8r_{max}$ considering a V4 neighborhood (i.e., four direct neighbors). If the radius $\rho = \sqrt{A_r/\pi}$ of the disk of same area A_r is larger than half of the displacement magnitude, then the velocity result is discarded.

Filters F_2, F_3, and F_4 are based on a steady-flow assumption. At a given velocity grid point, F_2 discards the outliers of the three standard deviation interval around the mean of the temporal distribution of the v_x and v_y velocity components (cf. Figure 6c). Filter F_3 is more drastic as it rejects all the measurements at a grid point if the coefficient of variation CV_p of the normal-to-transect velocity component v_p exceeds a given threshold (cf. Figure 6d). A threshold of 0.4 was used for this study. Filter F_4 also removes all the measurements at a grid point if the angles of the successive velocity vectors are too scattered (cf. Figure 6e), that is, if the circular variance var(θ) (Fisher, 1995) is greater than 0.25. The circular variance varies from 0 if all the vectors have the same angle, to 1 if the vectors are uniformly distributed on the unit circle.

Last, Filter F_5 is simply the computation of the time-median velocity at each grid point with more than 5 measurements. The time-median velocity is used instead of the time-average to be more robust to possible outliers.

Table 2
Details of the Assisted and Quasi-Automated Workflows Based on the Automatic Parameter Definition Tools P and the Filters F (cf. Text for Explanations)

LSPIV steps	Detail of the step	Assisted	Quasi-automated
Inputs	Image sequence extracted from video	User	User
	GCPs and transect data	User	User
	Manual spotting of displacements	–	User
	Surface coefficient α	User	User
Parameters	Ortho-image resolution	User	Auto (P_0)
	Grid points	Auto (P_1)	Auto (P_1)
	Size of the IA	User	Auto (40 pix.)
	Size of the SA	User	Auto (P_2)
	Framestep	Auto (P_3)	Auto (P_3)
Filtering (in sequence)	Median test	Auto (F_0)	Auto (F_0)
	Minimum correlation peak threshold r_{min}	Auto (0.3)	Auto (0.3)
	Minimum displacement magnitude threshold n_{min}	Auto (0.75 pix)	Auto (0.75 pix)
	Correlation peak width A_r filter	Auto (F_1)	Auto (F_1)
	Velocity temporal distribution filter	Auto (F_2)	Auto (F_2)
	Streamwise velocity dispersion filter	Auto (F_3)	Auto (F_3)
	Angular dispersion filter	Auto (F_4)	Auto (F_4)
	Time-median velocity field	Auto (F_5)	Auto (F_5)

3.3. New Workflows for LSPIV Discharge Computation

The proposed tools and filters are integrated into the LSPIV process implemented in Fudaa-LSPIV (cf. Figure 1), leading to two new workflows for discharge estimation: the "assisted LSPIV" and the "quasi-automated LSPIV" (cf. Table 2). The assisted LSPIV requires the user to set up the size of the IA, the SA and the surface coefficient α. The quasi-automated LSPIV only requires manual spotting and the surface coefficient α. For both workflows, filtering is applied in sequence according to the order presented in Table 2. For the quasi-automated workflow some manual spotting of the displacements are asked to the user in the area of higher velocities and lower velocities.

4. Results

4.1. The Sensitivity Analysis Based on the VGC2020

The discharge errors of the VGC2020 LSPIV measurements (as submitted by the participants) and the reprocessed LSPIV measurements are shown in Figure 7. Parameters external to the image velocimetry step, for example, α or the identification of the GCP coordinates, can have a significant impact on the discharge errors. The surface coefficient of video 3 has a specific value of $\alpha = 1.06$ due to the backwater created by a bridge downstream. This coefficient value can be obtained from the reference ADCP measurement. However, most of the participants used an underestimated value of $\alpha < 1$ (cf. Figure 1g). When the surface coefficient is forced to 1.06, the discharge measurements are greatly improved with errors less scattered and reduced by almost 10% (cf. $Q_{r|\alpha}$ of video 3 in Figure 7). Video 6 shows a high sensitivity to the image coordinates identified for each GCP. Discharges $Q_{r|GCPs}$ were reprocessed using GCPs whose image coordinates differ by several pixels from those of the Q_r analysis. This difference leads to significant variations of the discharge errors (cf. $Q_{r|GCPs}$ of video 6 in Figure 7). These variations are due to the poor spatial coverage of the 11 GCPs (cf. ortho-image in Figure 2) and to their difficult identification in the frame.

Most of the impacting parameters, for example, the framestep, the grid and the filters, are linked to the image-velocimetry analysis. The framestep and the filters are often sensitive parameters, especially for the videos with low apparent frame-to-frame displacements, for example, videos 1, 2, and 7. They have to be correctly set together to obtain a strong reduction of the discharge errors (cf. $Q_{r|framestep+filters}$ for videos 1, 2, and 7 in Figure 7).
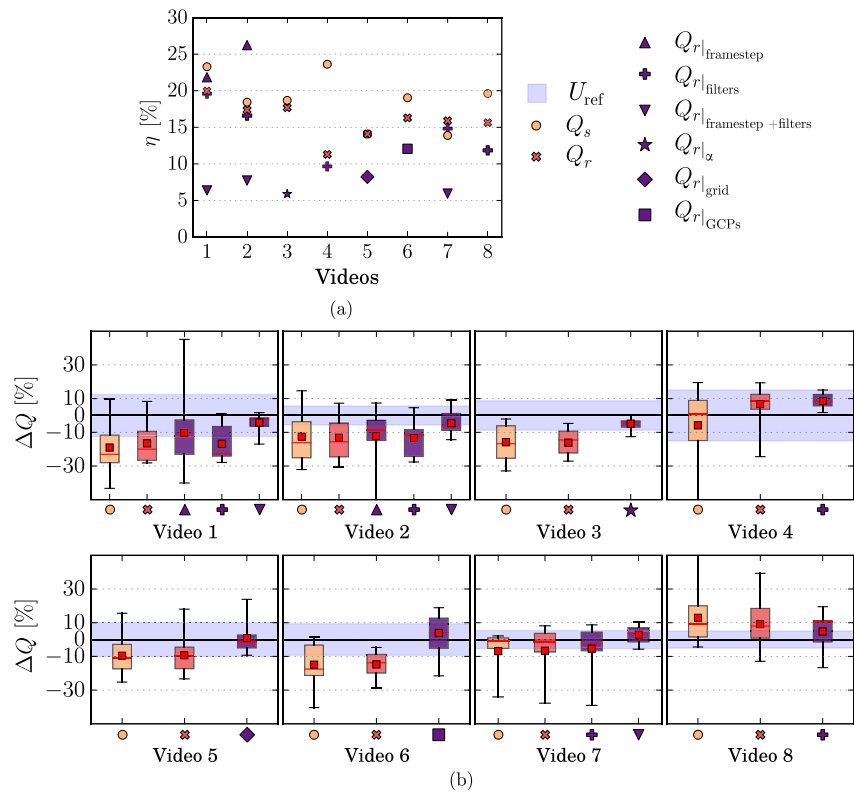
Figure 7. Discharge errors of the submitted data set Q_s, the replayed data set Q_r and the replayed data set with some parameters x forced $Q_{r|x}$, for the eight Video Globe Challenge 2020 videos: (a) Plot of the Root Mean Square Relative Error η; (b) Distribution of the percent errors ΔQ with U_{ref} the 95% uncertainty of the discharge reference (only the $Q_{r|x}$ data with the best results are shown for each video).

Indeed, forcing the framestep only without suitable filters usually does not improve the results, and may even deteriorate them (e.g. video 1 and 2). In these cases, the deterioration is caused by the larger time interval set to ensure large enough frame-to-frame displacements (i.e., larger than 3 pixels). As the time between successive frames increases, surface patterns can evolve further. Such evolution makes the surface patterns more difficult to identify on the next frame, leading oftenly to an erroneous measurement. Still, a sufficiently high framestep reduces the resolution uncertainty of the measured displacements and helps to segment spurious velocities from the actual flow velocities. Near zero velocities are mainly caused by error sources such as water transparency (e.g. video 1), occlusions (e.g. videos 2 and 7) or low seeding density in some areas (e.g. videos 2 and 7). They require a correct set of filters to be discarded, usually not sufficient in VGC2020 results.

The peak correlation filters and the velocity component filters are the only filters proposed in Fudaa-LSPIV. They could be inadequate to discard non zero spurious vectors in some situations. In video 8, the instable tracers generated by the rough surface are difficult to identify from frame to frame. This leads to noisy velocity fields difficult to filter. Video 5 shows poorly contrasted patterns near the right bank (cf. ortho-image in Figure 2) that lead to noisy velocity measurements with high correlation peaks. Many spurious vectors remain after applying the filters and cause an underestimation of the discharge measurements (cf. Q_s and Q_r of video 5 in Figure 7a). A solution employed by some participants was to use a truncated grid without points in the poorly contrasted area. The missing velocities in the truncated area are extrapolated at the discharge calculation step. A similar truncated grid is forced to all the participants and leads to a global improvement of the results (cf. $Q_{r|grid}$ of video 5 in Figure 7). This trick requires a high level of expertise. It highlights the shortcomings of the filters used and the impact of the grid points placement when error sources like occlusions, low tracers density and shadows are active. The distribution of the grid points also has a strong impact for video 4 due to the presence of trees hiding a large flow area around the transect. The largest errors of −63% and −65% observed in the submitted results are caused by near-zero velocities on measurement points placed in the areas

Table 3
Parameters Identified as the Most Impacting for the Eight Videos of the Video Globe Challenge 2020, Their Observed Impact on the Discharge Measurements and Setting Recommendations

Video	Impacting parameter(s)	Observed impact	Efficient setting
1	Framestep and filters	Strong and inter-dependent	Promote large displacements
2	Framestep and filters	Strong and inter-dependent	Promote large displacements
3	Surface coefficient	Strong	Estimate from ADCP measurement(s)
4	Grid	Limited to large errors	Set on visible areas
5	Grid and filters	Strong with a truncated grid	Remove grid points in poorly textured area
6	GCPs coordinates	Strong	Add GCPs around the flow
7	Framestep and filters	Strong and inter-dependent	Promote large displacements
8	Filters	Limited to large errors	Careful filter setting

covered by trees. These measurements replayed with a correct grid positioned in areas where the flow is visible are significantly improved with discharge errors decreased to 3% and −1% respectively (cf. Q_r of video 4 in Figure 7).

The conclusions on the parameter sensititivy for the eight videos of the VGC2020 are summarized in Table 3. Recommendations are also formulated to correctly set the other three parameters. For videos 1, 2 and 7, a large framestep can be used to promote large frame-to-frame displacements. This greatly helps the segmentation of near-zeros velocities and can lead to significant amelioration of the results with appropriate filters. The grid points in poorly textured areas can be removed to avoid spurious results, for example, video 5. However, this implies that the transect velocities will be extrapolated in these areas, assuming a linear variation of the local Froude number along the transect. Extrapolation error may occur if this assumption is not valid. The sensitive orthorectification of video 6 can only be improved by distributing more GCPs around the flow area.

4.2. Application of the Assisted LSPIV Workflow

The sensitivity analysis revealed that parameters such as the framestep, the grid points and the filters can have a strong impact on the LSPIV discharge measurements if they are not correctly set together. The analysis also showed that the peak correlation and velocity component filters are inadequate to discard spurious vectors in given situations. The assisted LSPIV workflow proposed in Section 3.3 was built to solve such problems. Best practice rules have been implemented for the setting of impacting parameters such as the framestep and the grid. Automatic and systematic filters have also been added. In this section, the assisted LSPIV workflow is applied to video 1 with a detailed analysis of the results (cf. Figure 8). The application uses the parameters of a participant who had a discharge error of $\Delta Q = -32\%$ to evaluate the benefit of the assisted workflow.

The input parameters are extracted from the participant report: orthorectification resolution of 0.016 m/pix, IA size of 26 pixels, SA dimensions of 26 pixels in the streamwise direction and 6 pixels in the other three directions and a surface coefficient α of 0.8. The grid is computed with the tool P_1. A framestep of 2 is determined by the tool P_3 and used to launch the LSPIV analysis. The raw measurements (cf. Figure 8a) contain several outliers and a non-negligible set of spurious near-zero velocities caused by the water transparency and the low seeding density in some areas. This impacts the time-median velocity field and leads to a larger underestimation of the discharge. The spatial coherency filter F_0 correctly removes the largest spurious vectors (cf. Figure 8b). A large amount of the spurious near zero velocities are discarded by the correlation peak width filter F_1 (cf. Figure 8c). Results are discarded by the temporal distribution filters F_2, F_3, and F_4 at several grid points on the right half of the flow (cf. Figure 8d). The filtered measurements look consistent and lead to a homogeneous time-median velocity field (cf. Figure 8d). The participant result is significantly improved with the assisted LSPIV from $\Delta Q = -32\%$ to $\Delta Q = -9.5\%$. With the default α value of 0.85 instead of 0.8 as used by the participant with no relevant justification, the discharge measurement matches well with the discharge reference with a relative error of $\Delta Q = -3.8\%$. This application confirms the benefit of a dense grid, sufficiently high frame-to-frame displacements and a drastic filtering strategy applied for LSPIV discharge estimation.
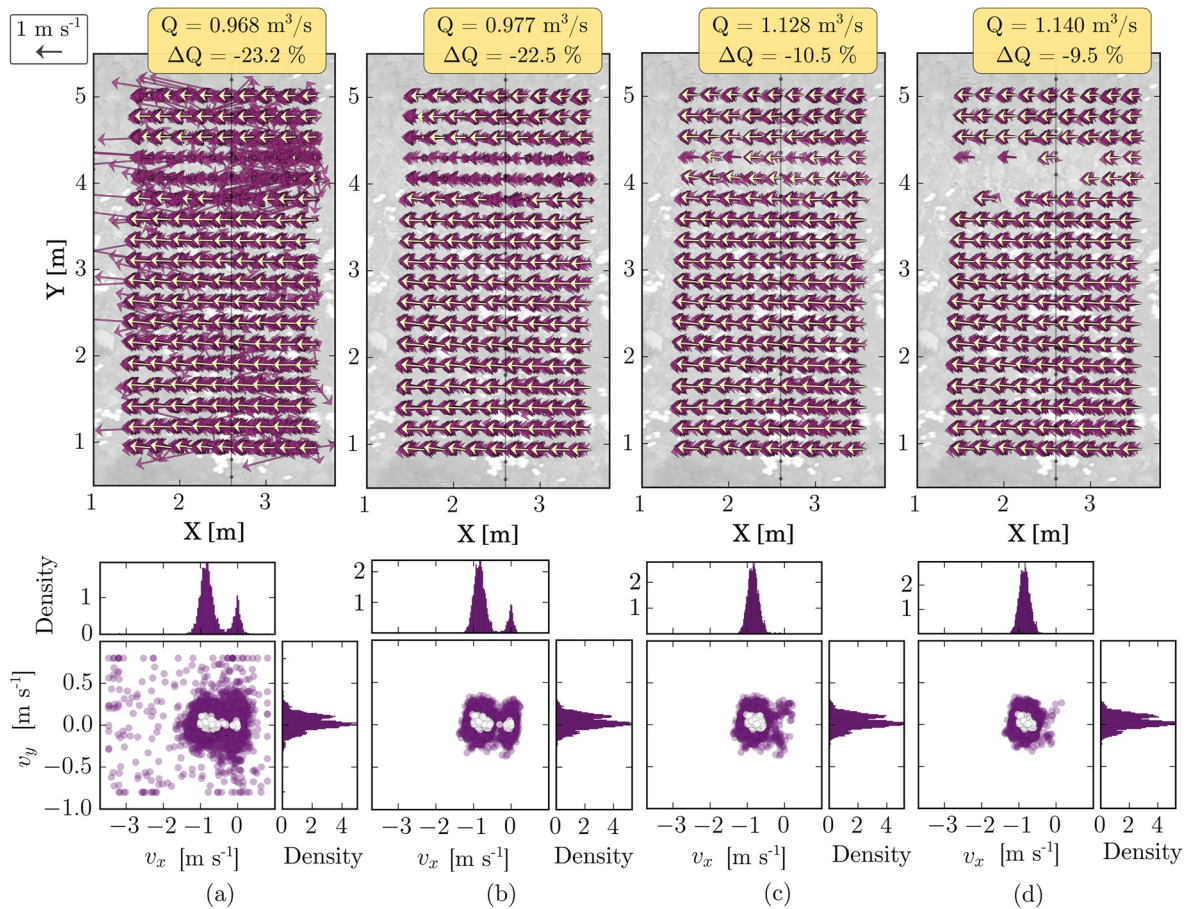
Figure 8. Application of sequential velocity filters to the results from a participant on video 1 of the VGC2020: (a) before filtering, (b) after spatial coherency filter F_0, (c) after correlation peak width filter F_1 and (d) after the last angular dispersion filter F_4. Top views show the velocity field (purple vectors), the time-median velocity field (white vectors) and the discharge measurement Q with the percent error ΔQ. The scatter plots and marginal distributions of the components v_x and v_y of the velocity vectors (purple) and the time-median velocity vectors (white) are also shown. The computational grid was defined automatically based on the transect (thin black dotted line) location. A framestep of 2 was automatically defined for the analysis.

4.3. Performance of the Assisted LSPIV on the VGC2020

The assisted LSPIV procedure is now applied to all the VGC2020 data set. The IA, SA, and surface coefficient are extracted from the LSPIV gauging reports. The video sequencing and GCPs are identical to those used for the other reprocessing (cf. Section 2.3). The grids defined automatically are shown in Supporting Information S1 attached to this article. The obtained discharge measurements are referred to as Q_{assist} and evaluated in Figure 9. Discharge measurements are also conducted by forcing the coefficient α to a correct value for all the participants. We established this correct α value for each video based on available information that has been made available to all participants such as ADCP-measured vertical velocity profiles or comments on wind conditions, channel roughness, backwater from a bridge, etc. (cf. e.g. Biggs et al., 2023; Costa et al., 2006; Hauet et al., 2018; Le Coz et al., 2010; Welber et al., 2016 on methods for estimating α). These discharge results allow to evaluate the measurement scatter without the effect of the user defined α coefficient. The discharge measurements obtained with the quasi-automated workflow and a correct value of α are also represented in Figure 9.

The automated parameters and filters greatly improve the discharge measurements with a very strong reduction of the scatter between participants. The interquartile range of the percent error distributions ranged from 6% to 24% with a mean value of 17% for the submitted results (cf. Figure 3a). With the assisted LSPIV and the user define α, it ranges from 0.8% to 13% with a mean value of 5% (cf. Figure 9b). The discharge errors induced by the image velocimetry are strongly reduced with the assisted LSPIV. Consequently, the surface coefficient α becomes the biggest contributor to the discharge measurements scatter. Indeed, with the assisted LSPIV and fixed α values, the interquartile range of the error distributions is reduced to 0.2%–3% with a mean value of 1.4% (cf.
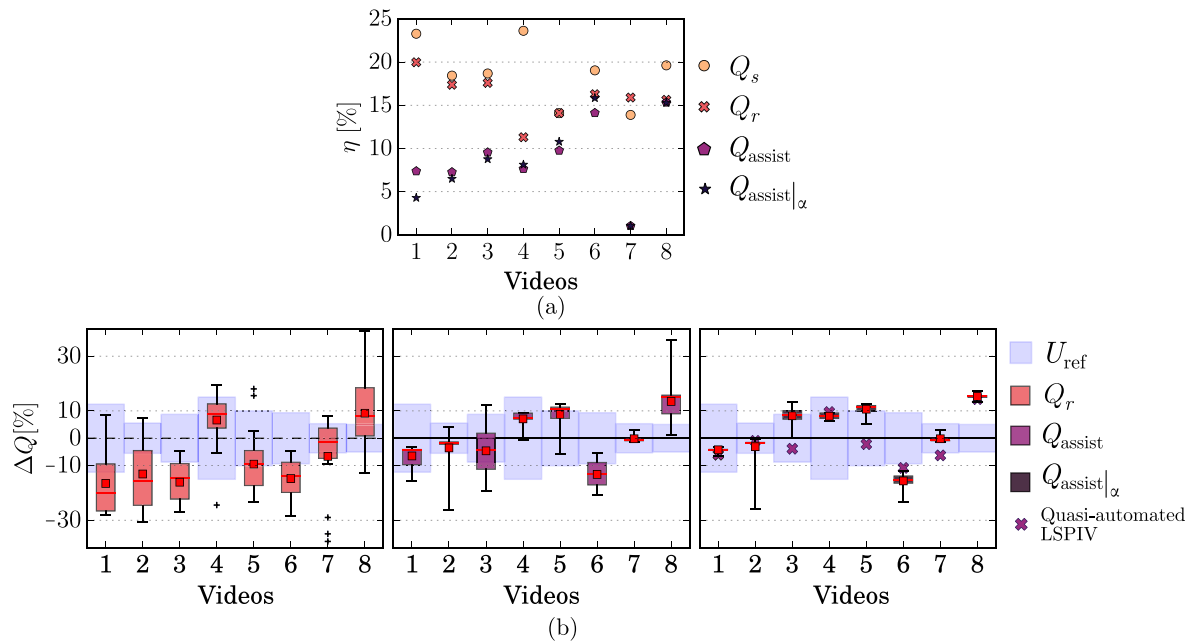
Figure 9. Discharge errors of the submitted data set Q_s, the replayed data set Q_r, the replayed data set with assisted Large Scale Particle Image Velocimetry (LSPIV) procedure Q_{assist}, with assisted LSPIV procedure and fixed α $Q_{assist|_\alpha}$ and with the quasi-automated LSPIV procedure for the eight Video Globe Challenge 2020 videos: (a) Root Mean Square Relative Error η; (b) Boxplots of the percent errors ΔQ with U_{ref} the 95% uncertainty of the discharge reference.

Figure 9b). The automated parameters and filters also reduce the measurements biases compared to the reference. The median of the percent errors ranged from −23% to 9% with a mean value of −9% (cf. Figure 3a). With the assisted LSPIV and the user define α, it ranges from −13% to 15% with a mean value of 1% (cf. Figure 9b). The biases observed for videos 4, 5, 6, and 8 are more significant now that the results are less scattered. For videos 3, 4, and 5 the results remain in good agreement with the discharge reference considering its 95% uncertainty.

The bias of video 6 is due to the orthorectification errors previously observed, as the GCPs of $Q_{assist.}$ are identical to those of Q_r. This bias is also observed in the submitted results Q_s and in the replayed results Q_r (cf. video 6 in Figure 9b).

Similar observations are made on the results of video 8 with a bias observed for discharges submitted Q_s, replayed Q_r and replayed with assistance Q_{assist} (cf. video 8 in Figure 7b). These biases can also be caused by orthorectification errors. The 4 GCPs used in this case are supposed to be at the same height as the river surface but they seem to be higher by about 0.2 m. This GCP elevation error may have a great impact on the orthorectification and velocity results due to the low viewing angle and the small width of the stream.

For video 4 the bias could be due to extrapolation errors. Nearly two thirds of the transect velocities are extrapolated due to occlusions by trees (cf. ortho-image of video 4 in Figure 2). In these areas the effect of the vegetation is not taken into account in the extrapolation of the velocities. This may explain the over-estimation observed for the replayed results Q_r and Q_{assist} of video 4 in Figure 9b. The positive bias caused by extrapolation errors could have been compensated by the underestimated velocities of the participants results Q_s due to inappropriate filters for instance (cf. Q_s of video 4 in Figure 7). Still, the discharge estimates remain in good agreement with the discharge reference considering its 95% uncertainty (cf. video 4, Figure 9b).

The discharge measurements obtained with the quasi-automated LSPIV are in good agreement with the reference (cf. Figure 9b). Overall, both assisted LSPIV and quasi-automated LSPIV show a strong improvement of the discharge measurements. The quasi-automated LSPIV can be used to obtain a reliable order of magnitude of the discharge and then be improved by adjusting the surface coefficient or the IA for instance.

5. Discussion

5.1. Benefits and Limits of Inter-Comparisons of Video-Based Streamgauging

Streamgauging intercomparisons have boosted the development of measurement tools by highlighting operating limits linked to the method or to the operator (e.g., Despax et al., 2019; Le Coz et al., 2016 for ADCP). In the proposed study, a video gauging intercomparison data set (VGC2020) allowed to investigate the operator effect due to data processing in LSPIV discharge measurement, to conduct a sensitivity analysis of the LSPIV method, and to evaluate assisted parameters and systematic filters for the LSPIV workflow. Such studies and evaluations are highly valuable in promoting the operational deployment of the technique. Still, several questions arise: is it possible to generalize the conclusion of the sensitivity analysis to all the measurement conditions? Is there a risk of over-fitting as the solutions proposed (parameter assistant tools and filters) were built and evaluated on this sample? How accurate are these conclusions in the context of reference measurements with potentially high uncertainties ? These limits are linked to the intercomparison data set. Ideally, the data set should be as large and as accurate as possible.

The VGC2020 data set used in this study offers a representative subset with various measurement conditions. This subset is more generic than the data sets used in other approaches of image-based hydrometry errors, for example, (Detert, 2021; Pizarro et al., 2020; Pumo et al., 2021). The VGC2020 data set is also interesting as it comes with discharge references and associated uncertainty, as opposed to other data sets, for example, (Perks et al., 2020). Several missing informations such as the user-defined grids and GCPs image coordinates could have been useful to the studies. For future intercomparisons, it would be beneficial to collect all measurement data (parameters, inputs, study files), to have a spatialized and accurate surface velocity reference, and possibly to impose several parameters to the participants such as the video sequencing, the GCPs or grid points in order to study the other parameters specifically. Realistic synthetic image generation methods, for example, (Bodart et al., 2022), can be used to build up a large data set with accurately known velocity reference.

In addition to the image and flow conditions, the profiles of the participants to the intercomparison also contribute to the variability of the results. Therefore, it would be interesting to document and quantify the type, experience and knowledge of the participants through criteria as objective as possible. Even though the VGC2020 exercise does not allow for a comprehensive study of participant profiles, some participants systematically provided better or poorer results than the average (with no obvious relation to their level of experience), while others improved their performance after processing their first videos. Participants using other software than Fudaa-LSPIV and other techniques than LSPIV were not numerous enough to extend the intercomparison analysis beyond the software-specific limitations and particularities. Ideally, the same exercise would be executed with multiple software and techniques to evaluate which sources of errors are specific and which ones are generic to all image-based surface velocity streamgauging techniques.

5.2. Reducing the Sensitivity of LSPIV

The sensitivity of the LSPIV method, at least as implemented in Fudaa-LSPIV, is mainly linked to the large freedom of parameter settings left to the user. For the image-based velocimetry step, the users have to specify many parameters including the location of the measurement points (grid), the size of the surface patterns to be tracked (IA), their possible displacements (SA) and the appropriate filtering. This requires a substantial expertise from the user and can lead to large errors if inappropriate choices are made. The sensitivity of the velocity results to the framestep, or time-interval, was already noticed by Pumo et al. (2021) and the impacts of the orthorectification and filters were also noticed by Detert (2021). Several methods limit this sensitivity by using automated frameworks such as automatic setting of the measurement points in textured areas, for example, in FlowVelo (Eltner et al., 2019) and KLT-IV (Perks, 2020), by using specific assumptions such as unidimensional and temporally coherent flow in STIV (Fujita et al., 2007), or by asking manual inputs from the user such as identifying tracer passage on spatio-temporal images in STIV. In this paper we propose to apply similar constraints to the LSPIV workflow resulting in an assisted LSPIV and quasi-automated LSPIV frameworks. This leads to a significant reduction of the LSPIV variability and a significant improvement of the LSPIV performances on the VGC2020 data set. Some of the tools proposed were already employed by other methods based on LSPIV, for example, local filters used systematically in SSIV (Leitão et al., 2018). The assisted LSPIV and quasi-automated LSPIV frameworks offer a great potential for discharge measurements as reliable results could be obtained with less user parametrization. The proposed automatic parameter definition scheme can still gain in robustness by valorizing simple user inputs or assumptions instead of using automatic computations. For instance, manual spotting of the

velocities in various areas (i.e., low to high velocity area) can be used to determine the framstep instead of the preliminary LSPIV computation proposed.

Overall, extensive filtering is mandatory to obtain reliable and robust measurements in image velocimetry. The sequence of filters proposed in this paper gave promising results. Especially, filter $F1$ (correlation peak width) is designed to discard spurious velocity results due to poor tracer quality and density, and it proves to be efficient. Indeed, image velocimetry always rely on visible tracers of the flow movement (or "optical flow," cf. Bodart et al., 2022) and a great amount of the observed errors are due to the lack of tracers (Dal Sasso et al., 2020; Iverson Italo Siebert & Bleninger, 2023; Pumo et al., 2021) and/or the presence of tracers moving with velocity different from the water velocity, such as gravity waves (Dolcetti et al., 2020). But many other filters can be implemented such as the PPSR (Li & Yan, 2022) or the seeding density metrics (Pizarro et al., 2020) for instance. From our observations, a drastic filtering strategy is beneficial to the image velocimetry measurement. We noticed a significant sensitivity of the filters efficiency to their order of application. A good balance has to be found to ensure that spurious results would be discarded without removing too much of the correct ones. The user expertise will always be needed to validate the results, even with automated procedures. In this context, relevant metrics and data representations like the density analysis proposed in Figure 8 should be used to assist the decision process.

5.3. Toward Robust LSPIV Measurements

The analysis showed that the most sensitive parameters and their impacts on the discharge measurement vary from case to case. These variations are closely linked to the error sources, for example, occlusions, low seeding densities or water transparency. This means that the sensitivity of the image velocimetry strongly depends on the measurement conditions and also that without specific error sources, the parameter sensitivity may be strongly reduced. To avoid large errors, best practice rules for the data acquisition, processing and post-processing should be defined and followed. For instance, this study shows that automatizing best practice rules for data processing strongly reduces large measurement errors. In addition, to reach robust LSPIV measurements, guidelines for QA and criteria for QC have to be formulated.

Several guidelines have already been formulated by Detert (2021), WaMSTeC(2021) for the data acquisition. They can be complemented with our observations. We observed that not only the amount of GCPs but also their spatial distribution in the scene is of importance for a correct 3D orthorectification. Ideally, the surveyed points should not be grouped but rather scattered throughout the region of interest. It is also worth noting that GCPs have to be located close to the water surface (compared to Δz between camera and water surface) for 2D orthorectification. Several procedures can be used afterward to evaluate the sensitivity and related uncertainties of the 3D orthorectification, for example, (Le Coz, Renard, et al., 2021; Schweitzer & Cowen, 2022). The surface coefficient remains an important concern for contactless discharge measurements. Recommendations can already be found in the literature, for example, $\alpha = 0.85$ for natural rivers and $\alpha = 0.9$ for artificial concrete channels (Costa et al., 2006; Hauet et al., 2018; Le Coz et al., 2010; Welber et al., 2016). From our observations, we suggest to pay attention to specific hydraulic situations such as backwater or wind effects which can influence the surface coefficient.

Quality criteria can be used in the context of QC, to assist the evaluation of the measurement toward quality assessment. In the context of discharge measurement, several quality criteria are already formulated in the ISO748 - Hydrometry standard (ISO, 2021b). Additional criteria can be proposed for image-based hydrometry. The viewpoint can be evaluated: high enough viewing angle? No camera shaking influencing the view? The tracer density throughout the region of interest can be evaluated either with a subjective score or with specific metrics. The metrics could be the image texture as used by Li and Yan (2022), the seeding density metric (Pizarro et al., 2020) or, for LSPIV measurements, the correlation peak width as proposed in this paper. The distribution of the velocity results throughout the region of interest can be evaluated. For instance, the differential entropy (Cover & Thomas, 2005) could be used to identify quasi uniform distributions of the measurements due to very noisy measurements. The coherency of the transect velocities can be evaluated: low enough amount of extrapolated velocities? Consistent variations of the local Froude number across the transect?

6. Conclusion

A video gauging intercomparison, the VGC2020 (Le Coz, Hauet, & Despax, 2021), was analyzed to quantify the operator effect due to data processing in LSPIV discharge measurements. The measurements from 15 to 23 participants applying the Fudaa-LSPIV software to the eight videos of the VGC2020 were replayed and studied.

A significant operator effect was noticed with a strong scatter of the discharge measurements provided by the participants. This intercomparison exercise is representative of real practice, and the results are meaningful in showing that instructions and training are not enough to prevent a lot of users from making mistakes and getting inaccurate discharge results using LSPIV. The framestep, that is, the video sub-sampling factor, the computational grid, and the velocity filters often appear to be sensitive parameters. An inter-dependency between these parameters was noticed which means that they have to be adjusted jointly to reduce the discharge error. From our observations, these parameters had a stronger impact than the image processing settings (IA and SA). In specific cases the surface coefficient α and the GCPs used for the orthorectification also had a strong impact on the discharge measurements.

Based on these observations, several tools were proposed to reduce the LSPIV discharge variability due to the operator effect. The objective was first to automatically set as many parameters as possible to reduce the user inputs, and second to ensure robust and consistent measurement with systematic and automated filters. Parameter automatic definition was proposed for the orthorectification resolution (P_0), the grid points (P_1), the size of the SA (P_2) and the framestep (P_3), based on the available data (e.g., GCPs, transect) and simple user inputs (e.g., manual spotting of a few displacements). In sequence, the systematic filtering procedure includes the median test (Westerweel & Scarano, 2005) (F_0), a minimum correlation threshold, a minimum pixel displacement threshold, a maximum threshold on the ratio between the correlation peak width and the displacement (F_1), a filtering of the outliers of the velocity temporal distribution at a point (F_2) and a filtering of the grid points with either high streamwise velocity dispersion (F_3) or high angular dispersion (F_4) and the determination of the time-median velocity at a point (F_5). With this assisted LSPIV workflow, only the video sequencing, GCPs, IA, SA, surface coefficient and transect information have to be set by the user. These tools were not available to the participants who had to set the proper parameters and filters based on their own expertise, through the existing, limited Fudaa-LSPIV options. To assess the overall improvement of the results of all the participants if such automatic tools had been available to them, this workflow was applied to the VGC2020 using the IA, SA and surface coefficient from the participants gauging reports. This led to a significant improvement of the discharge measurements. The dispersion of the inter-participant discharge errors across the videos was strongly reduced with a mean inter-quartile range of 5% and a mean median error of +1%. A quasi-automated LSPIV framework with the smallest user input (only video sequencing, GCPs and manual spotting of the displacements) was also evaluated and provided consistent results in agreement with the discharge reference and its uncertainty.

This study highlights the benefit of intercomparisons for the development of outdoor image velocimetry, as it was made for the ADCP earlier. Such exercise can be applied to the various image-based methods to better characterize their advantages and drawbacks in given situations and stimulate methodological developments. For more precise studies, realistic synthetic images with exact velocity reference (Bodart et al., 2022) may help to better evaluate the measured velocity field in the presence of specific error sources.

The results of the assisted LSPIV are promising for the operational deployment of LSPIV for discharge measurement. From the observations on the VGC2020, reliable results can be obtained with the assisted framework even with a reduced experience from the user. This is an important progress for generalizing the access to the method. These tools may be implemented in LSPIV software tools, such as Fudaa-LSPIV. Still, as noted by Detert (2021), image velocimetry is also sensitive to the measurement setup, the data acquisition and the camera calibration. These aspects can only be treated with the elaboration of standards, guidelines, dedicated training and homogeneous procedures for uncertainty estimation. Finally, despite the progress of contacless methods for surface velocimetry (radar, imagery), several sources of errors still impact the discharge measurement during flood events such as riverbed evolution, vertical velocity distribution and water level estimation. An operating method for computing discharge uncertainty still has to be developed, reflecting these sources of uncertainty.

Data Availability Statement

The data set of the VGC2020 intercomparison can be found at https://doi.org/10.57745/KVNIHX (Bodart et al., 2023). This data set contains the videos, files for the LSPIV processing (GCPs, bathymetry), the discharge references and the results submitted by the participants (LSPIV parameters from the gauging reports and discharge measurements). The Fudaa-LSPIV software and its user manual can be found at https://forge.irstea.fr/projects/fudaa-lspiv/files. The sources of the Fudaa-LSPIV interface can be found at https://gitlab.com/fudaa/fudaa-lspiv with a GNU GPL v2 license. The sources of the Fudaa-LSPIV solvers can be found at https://gitlab.irstea.fr/image_velocimetry/velocimetry_solver with a GNU LGPL v3 license.

References

Adrian, R. J. (1991). Particle-imaging techniques for experimental fluid mechanics. *Annual Review of Fluid Mechanics*, *23*(1), 261–304. https://doi.org/10.1146/annurev.fl.23.010191.001401

Bentley, J. L. (1975). Multidimensional binary search trees used for associative searching. *Communications of the ACM*, *18*(9), 509–517. https://doi.org/10.1145/361002.361007

Biggs, H., Holwerda, N., Smart, G., Doyle, M., McDonald, M., & Ede, M. (2021). *River discharge from surface velocity measurements (technical report no. 2021196CH)*. NIWA.

Biggs, H., Smart, G., Doyle, M., Eickelberg, N., Aberle, J., Randall, M., & Detert, M. (2023). Surface velocity to depth-averaged velocity—A review of methods to estimate alpha and remaining challenges. *Water*, *15*(21), 3711. https://doi.org/10.3390/w15213711

Bodart, G., Le Coz, J., Jodeau, M., & Hauet, A. (2022). Synthetic River flow videos for evaluating image-based velocimetry methods. *Water Resources Research*, *58*(12), e2022WR032251. https://doi.org/10.1029/2022WR032251

Bodart, G., Le Coz, J., Jodeau, M., & Hauet, A. (2023). Video globe challenge 2020 dataset. https://doi.org/10.57745/KVNIHX

Brevis, W., Niño, Y., & Jirka, G. H. (2011). Integrating cross-correlation and relaxation algorithms for particle tracking velocimetry. *Experiments in Fluids*, *50*(1), 135–147. https://doi.org/10.1007/s00348-010-0907-z

Callède, J., Guyot, J. L., Ronchail, J., Seyler, F., Guimarães, V., & de Oliveira, E. (2003). Amazon river discharge variability at the Obidos gauging station during the last century, 9224. In *EGS-AGU—EUG joint assembly ADS*. Retrieved from https://ui.adsabs.harvard.edu/abs/2003EAEJA…9224C

Costa, J. E., Cheng, R. T., Haeni, F. P., Melcher, N., Spicer, K. R., Hayes, E., et al. (2006). Use of radars to monitor stream discharge by noncontact methods. *Water Resources Research*, *42*(7), W07422. https://doi.org/10.1029/2005WR004430

Costa, J. E., Spicer, K. R., Cheng, R. T., Haeni, F. P., Melcher, N. B., Thurman, E. M., et al. (2000). Measuring stream discharge by non-contact methods: A proof-of-concept experiment. *Geophysical Research Letters*, *27*(4), 553–556. https://doi.org/10.1029/1999GL006087

Cover, T. M., & Thomas, J. A. (2005). Differential entropy. In *Elements of information theory* (pp. 243–259). John Wiley & Sons, Ltd. https://doi.org/10.1002/047174882X

Creutin, J. D., Muste, M., Bradley, A. A., Kim, S. C., & Kruger, A. (2003). River gauging using PIV techniques: A proof of concept experiment on the Iowa river. *Journal of Hydrology*, *277*(3), 182–194. https://doi.org/10.1016/S0022-1694(03)00081-7

Dal Sasso, S. F., Pizarro, A., & Manfreda, S. (2020). Metrics for the quantification of seeding characteristics to enhance image velocimetry performance in rivers. *Remote Sensing*, *12*(11), 1789. https://doi.org/10.3390/rs12111789

Despax, A., Le Coz, J., Hauet, A., Mueller, D. S., Engel, F. L., Blanquart, B., et al. (2019). Decomposition of uncertainty sources in acoustic Doppler current profiler streamflow measurements using repeated measures experiments. *Water Resources Research*, *55*(9), 7520–7540. https://doi.org/10.1029/2019WR025296

Despax, A., Le Coz, J., Mueller, D. S., Hauet, A., Calmel, B., Pierrefeu, G., et al. (2023). Validation of an uncertainty propagation method for moving-boat acoustic doppler current profiler discharge measurements. *Water Resources Research*, *59*(1), e2021WR031878. https://doi.org/10.1029/2021WR031878

Detert, M. (2021). How to avoid and correct biased riverine surface image velocimetry. *Water Resources Research*, *57*(2), e2020WR027833. https://doi.org/10.1029/2020WR027833

Dolcetti, G., Hortobágyi, B., Perks, M., & Tait, S. (2020). The effect of surface gravity waves on the measurement of river surface velocity. In *River flow 2020: 10th conference on fluvial hydraulics*. CRC Press (Taylor & Francis). Retrieved from https://eprints.whiterose.ac.uk/165812/

Eltner, A., Sardemann, H., & Grundmann, J. (2019). Flow velocity and discharge measurement in rivers using terrestrial and UAV imagery. In *Rivers and lakes/remote sensing and GIS*. https://doi.org/10.5194/hess-2019-289

Fisher, N. I. (1995). *Statistical analysis of circular data*. Cambridge University Press.

Foley, J. D., & Van Dam, A. (1982). *Fundamentals of interactive computer graphics*. Addison-Wesley Longman Publishing Co., Inc.

Fujita, I., Muste, M., & Kruger, A. (1998). Large-scale particle image velocimetry for flow analysis in hydraulic engineering applications. *Journal of Hydraulic Research*, *36*(3), 397–414. https://doi.org/10.1080/00221689809498626

Fujita, I., Watanabe, H., & Tsubaki, R. (2007). Development of a non-intrusive and efficient flow monitoring technique: The space-time image velocimetry (STIV). *International Journal of River Basin Management*, *5*(2), 105–114. https://doi.org/10.1080/15715124.2007.9635310

González-Castro, J. A., & Muste, M. (2007). Framework for estimating uncertainty of ADCP measurements from a moving boat by standardized uncertainty analysis. *Journal of Hydraulic Engineering*, *133*(12), 1390–1410. https://doi.org/10.1061/(ASCE)0733-9429(2007)133:12(1390)

Hauet, A., Florvaag-Dybvik, K., Dahl, M.-P. J., Kvernhaugen, F. T., Møen, K. M., & Sentlinger, G. (2020). Uncertainty of discharge measurement using salt dilution (technical report no. EGU2020-4661). In *Copernicus meetings*. https://doi.org/10.5194/egusphere-egu2020-4661

Hauet, A., Kruger, A., Krajewski, W. F., Bradley, A., Muste, M., Creutin, J.-D., & Wilson, M. (2008). Experimental system for real-time discharge estimation using an image-based method. *Journal of Hydrologic Engineering*, *13*(2), 105–110. https://doi.org/10.1061/(ASCE)1084-0699(2008)13:2(105)

Hauet, A., Morlot, T., & Daubagnan, L. (2018). Velocity profile and depth-averaged to surface velocity in natural streams: A review over a large sample of rivers. In *E3S web of conferences, 40, 06015*. EDP Sciences. https://doi.org/10.1051/e3sconf/20184006015

ISO. (2021a). ISO 24578:2021—Hydrometry—Acoustic Doppler profiler—Method and application for measurement of flow in open channels from a moving boat. Retrieved from https://www.iso.org/standard/70758.html

ISO. (2021b). ISO 748:2021—Hydrometry—Measurement of liquid flow in open channels—Velocity area methods using point velocity measurements. Retrieved from https://www.iso.org/cms/render/live/en/sites/isoorg/contents/data/standard/07/27/72754.html

Iverson Italo Siebert, M. M., & Bleninger, T. (2023). Low-cost surface particle image velocimetry for hydraulic model studies. *Journal of Applied Water Engineering and Research*, *11*(1), 104–116. https://doi.org/10.1080/23249676.2022.2084165

Jodeau, M., Hauet, A., Le Coz, J., Faure, J.-B., & Bodart, G. (2022). Fudaa-LSPIV user manual (v 1.9.2). Retrieved from https://forge.irstea.fr/projects/fudaa-lspiv/files

Jodeau, M., Hauet, A., Paquier, A., Coz, J., & Dramais, G. (2008). Application and evaluation of LS-PIV technique for the monitoring of river surface velocities in high flow conditions. *Flow Measurement and Instrumentation*, *19*(2), 117–127. https://doi.org/10.1016/j.flowmeasinst.2007.11.004

Kiang, J. E., Gazoorian, C., McMillan, H., Coxon, G., Le Coz, J., Westerberg, I. K., et al. (2018). A comparison of methods for streamflow uncertainty estimation. *Water Resources Research*, *54*(10), 7149–7176. https://doi.org/10.1029/2018WR022708

Kim, Y., Muste, M., Hauet, A., Bradley, A., Weber, L., & Koh, D. (2007). Uncertainty analysis for LSPIV in-situ velocity measurements. In *Proceedings 32nd IAHR congress, Venice, Italy*.

Le Coz, J. (2017). Quantifying discharges and fluxes of matters in rivers (thesis, Habilitation à Diriger des Recherches, Université Grenoble Alpes) (p. 92). Retrieved from https://hal.inrae.fr/tel-02606946

Le Coz, J., Blanquart, B., Pobanz, K., Dramais, G., Pierrefeu, G., Hauet, A., & Despax, A. (2016). Estimating the uncertainty of streamgauging techniques using in situ collaborative interlaboratory experiments. *Journal of Hydraulic Engineering*, *142*(7), 04016011. https://doi.org/10.1061/(ASCE)HY.1943-7900.0001109

Le Coz, J., Hauet, A., & Despax, A. (2021). The video Globe Challenge 2020, a video streamgauging race during the Covid-19 lockdown (technical report no. EGU21-2116). In *Copernicus Meetings*. https://doi.org/10.5194/egusphere-egu21-2116

Le Coz, J., Hauet, A., Pierrefeu, G., Dramais, G., & Camenen, B. (2010). Performance of image-based velocimetry (LSPIV) applied to flash-flood discharge measurements in Mediterranean rivers. *Journal of Hydrology*, *394*(1), 42–52. https://doi.org/10.1016/j.jhydrol.2010.05.049

Le Coz, J., Jodeau, M., Hauet, A., Marchand, B., & Le Boursicaud, R. (2014). Image-based velocity and discharge measurements in field and laboratory river engineering studies using the free Fudaa-LSPIV software. In *River flow 2014* (pp. 1961–1967). https://doi.org/10.1201/b17133-262

Le Coz, J., Renard, B., Vansuyt, V., Jodeau, M., & Hauet, A. (2021). Estimating the uncertainty of video-based flow velocity and discharge measurements due to the conversion of field to image coordinates. *Hydrological Processes*, *35*(5), e14169. https://doi.org/10.1002/hyp.14169

Leitão, J. P., Peña-Haro, S., Lüthi, B., Scheidegger, A., & Moy de Vitry, M. (2018). Urban overland runoff velocity measurement with consumer-grade surveillance cameras and surface structure image velocimetry. *Journal of Hydrology*, *565*, 791–804. https://doi.org/10.1016/j.jhydrol.2018.09.001

Lennermark, M., & Hauet, A. (2022). Developing a post-processing software for ADCP discharge measurement piloted by an international and inter-agency group: A unique, ambitious experience… and one that works! (technical report no. EGU22-9379). In *Copernicus meetings*. https://doi.org/10.5194/egusphere-egu22-9379

Li, L., & Yan, H. (2022). A robust filtering algorithm based on the estimation of tracer visibility and stability for large scale particle image velocimetry. *Flow Measurement and Instrumentation*, *87*, 102204. https://doi.org/10.1016/j.flowmeasinst.2022.102204

Moore, S. A., Jamieson, E. C., Rainville, F., Rennie, C. D., & Mueller, D. S. (2017). Monte Carlo approach for uncertainty analysis of acoustic Doppler current profiler discharge measurement by moving boat. *Journal of Hydraulic Engineering*, *143*(3), 04016088. https://doi.org/10.1061/(ASCE)HY.1943-7900.0001249

Mueller, D. S. (2016). *QRev–Software for computation and quality assurance of Acoustic Doppler current profiler moving-boat streamflow measurement: Technical manual for version 2.8* (Vol. 2016). US Department of the Interior, US Geological Survey.

Mueller, D. S., Wagner, C. R., Rehmel, M. S., Oberg, K. A., & Rainville, F. (2013). Measuring discharge with acoustic Doppler current profilers from a moving boat (USGS Numbered Series No. 3-A22). In *Measuring discharge with acoustic Doppler current profilers from a moving boat Series: Techniques and Methods*. U.S. Geological Survey. https://doi.org/10.3133/tm3A22

Muste, M., Fujita, I., & Hauet, A. (2008). Large-scale particle image velocimetry for measurements in riverine environments. *Water Resources Research*, *44*(4), W09502. https://doi.org/10.1029/2008WR006950

Oberg, K., & Mueller, D. S. (2007). Validation of streamflow measurements made with acoustic doppler current profilers. *Journal of Hydraulic Engineering*, *133*(12), 1421–1432. https://doi.org/10.1061/(ASCE)0733-9429(2007)133:12(1421)

Oyallon, E., & Rabin, J. (2015). An analysis of the SURF method. *Image Processing On Line*, *5*, 176–218. https://doi.org/10.5201/ipol.2015.69

Pearce, S., Ljubičić, R., Peña-Haro, S., Perks, M., Tauro, F., Pizarro, A., et al. (2020). An evaluation of image velocimetry techniques under low flow conditions and high seeding densities using unmanned aerial systems. *Remote Sensing*, *12*(2), 232. https://doi.org/10.3390/rs12020232

Perks, M. T. (2020). KLT-IV v1.0: Image velocimetry software for use with fixed and mobile platforms. *Geoscientific Model Development*, *13*(12), 6111–6130. https://doi.org/10.5194/gmd-13-6111-2020

Perks, M. T., Dal Sasso, S. F., Hauet, A., Jamieson, E., Le Coz, J., Pearce, S., et al. (2020). Towards harmonisation of image velocimetry techniques for river surface velocity observations. *Earth System Science Data*, *12*(3), 1545–1559. https://doi.org/10.5194/essd-12-1545-2020

Perks, M. T., Russell, A. J., & Large, A. R. G. (2016). Technical note: Advances in flash flood monitoring using unmanned aerial vehicles (UAVs). *Hydrology and Earth System Sciences*, *20*(10), 4005–4015. https://doi.org/10.5194/hess-20-4005-2016

Pizarro, A., Dal Sasso, S. F., Perks, M., & Manfreda, S. (2020). Spatial distribution of tracers for optical sensing of stream surface flow. In *Engineering Hydrology/Instruments and observation techniques*. https://doi.org/10.5194/hess-2020-188

Pumo, D., Alongi, F., Ciraolo, G., & Noto, L. V. (2021). Optical methods for river monitoring: A simulation-based approach to explore optimal experimental setup for LSPIV. *Water*, *13*(3), 247. https://doi.org/10.3390/w13030247

Rantz, S. (1982). *Measurement and computation of streamflow (Volume 1: Measurement of stage and discharge, water-supply paper 2175)*. U. S. Geological Survey.

Rousseau, G. (2019). *Turbulent flows over rough permeable beds in mountain rivers: Experimental insights and modeling (Unpublished doctoral dissertation)*. EPFL.

Rowe, F., & Young, J. (1979). An Ocean current profiler using Doppler sonar. In *Oceans '79* (pp. 292–297). https://doi.org/10.1109/OCEANS.1979.1151265

Rozos, E., Dimitriadis, P., Mazi, K., Lykoudis, S., & Koussis, A. (2020). On the uncertainty of the image velocimetry method parameters. *Hydrology*, *7*(3), 65. https://doi.org/10.3390/hydrology7030065

Schweitzer, S. A., & Cowen, E. A. (2022). A method for analysis of spatial uncertainty in image based surface velocimetry. *Frontiers in Water*, *4*, 744278. https://doi.org/10.3389/frwa.2022.744278

Simpson, M. R., & Oltmann, R. N. (1993). Discharge measurement system using an acoustic Doppler current profiler with applications to large rivers and estuaries. In *U.S. Geological survey water supply paper 2395* (p. 32).

Thielicke, W., & Stamhuis, E. (2014). PIVlab—Towards user-friendly, affordable and accurate digital particle image velocimetry in MATLAB. *Journal of Open Research Software*, *2*(1), e30. https://doi.org/10.5334/jors.bl

Tomar, S. (2006). Converting video formats with FFmpeg. *Linux Journal*, *2006*(146), 10.

USGS. (2022). Guidelines for the collection of video for large Scale Particle velocimetry (LSPIV). Retrieved from https://my.usgs.gov/confluence/pages/viewpage.action?pageId=546865360

WaMSTeC. (2021). Application of surface velocity methods for velocity and open channel discharge measurements. In *National industry guidelines for hydrometric monitoring (Australian government, Bureau of Meteorology ed.)* (Vol. 11).

Welber, M., Le Coz, J., Laronne, J. B., Zolezzi, G., Zamler, D., Dramais, G., et al. (2016). Field assessment of noncontact stream gauging using portable surface velocity radars (SVR). *Water Resources Research*, *52*(2), 1108–1126. https://doi.org/10.1002/2015WR017906

Westerweel, J., & Scarano, F. (2005). Universal outlier detection for PIV data. In *Experiments in fluids: Experimental methods and their applications to fluid flow* (Vol. 39, pp. 1096–1100). https://doi.org/10.1007/s00348-005-0016-6

WMO. (2010). *Manual on stream gauging, Vol. I: Fieldwork*. World Meteorological Organization (WMO).

Zhang, Z. (2000). A flexible new technique for camera calibration. *IEEE Transactions on Pattern Analysis and Machine Intelligence*, *22*(11), 1330–1334. https://doi.org/10.1109/34.888718